FABRICATION AND INVESTIGATION OF GaN NANOSTRUCTURES AND THEIR APPLICATIONS IN AMMONIA GAS SENSING

BEH KHI POAY

UNIVERSITI SAINS MALAYSIA

2015

FABRICATION AND INVESTIGATION OF GaN NANOSTRUCTURES AND THEIR APPLICATIONS IN AMMONIA GAS SENSING

by

BEH KHI POAY

Thesis submitted in fulfillment of the requirements for the Degree of Doctor of Philosophy

July 2015

ACKNOWLEDGEMENTS

First and foremost I would like to thank my supervisor, Dr. Yam Fong Kwong for offering me this project, which was under Research University (RU) grant scheme (1001/PFIZIK/811155). Next, I'm grateful to have Professor Zainuriah Hassan as my co-supervisor; both she and Dr. Yam have provided ample guidance and supports for me throughout these years. Then, I would like to thank the Institute of Post-graduate Studies (IPS) for offering me USM Fellowship award, USM-RU-PRGS (grant, 1001/PFIZIK/843087), and courses that supported my studies.

It is an honour in being a student from School of Physics, moreover member of Nano-Optoelectronics Research (N.O.R.) Laboratory. I would to thank all of the staffs for providing me support in many ways, such as characterizations, instrumentation assistance, and so on. In addition, I would like to express my sincere appreciation to Assoc. Prof. Dr. Mutharasu Devarajan and Dr. Norzaini Zainal for showing tremendous interests in this project.

Throughout my years, many challenges were faced. I'm fortunate to have Mr. Tneh Sau Siong, my senior, in mentoring me. Aside from that, I sincerely thank Ms. Ng Siow Woon for helping me in many ways. She is a dedicated person who showed me the spirit of "never give up".

I'm would like to thank my parents, Mr. Beh Kean Leng and Mdm. Leong Lai Ying for their supports and cares towards me since childhood. Additionally, I'm grateful for them to share their work experiences in semiconductor field of which I'm currently on. Lastly, I sincerely thank all those whose name not being mentioned here, for them who have helped me in many ways.

TABLE OF CONTENTS

PAGE

ACKNOWLEDGEMENT ii

TABLE OF CONTENT iii

LIST OF TABLES viii

LIST OF FIGURES ix

LIST OF ABBREVIATIONS xiv

LIST OF SYMBOLS xvii

LIST OF PUBLICATIONS xix

ABSTRAK xxii

ABSTRACT xxiv

CHAPTER 1 – INTRODUCTION

1.1 The Background of Gallium Nitride 1

1.2 Nanostructured GaN and NH_3 Gas Sensing 2

1.3 Research Goals and Novelties 4

1.4 Organization of Thesis Chapters 5

CHAPTER 2 – LITERATURE REVIEW

2.1 Introductions to GaN Nanowires 7

2.2 The Chemistry of GaN-related Precursors 14

2.3 The Growth Modes of GaN Nanowires 17

2.4 General Characteristics of GaN Nanowires 19

2.5 Porous GaN (PGaN) Fabrication Process 21

2.6 Introduction to NH_3 Gas Sensor 24

2.7 Summary 26

CHAPTER 3 – MATERIALS AND METHODOLOGIES

3.1 The Essential Materials 28

3.1.1 Materials for GaN-Ga_2O_3 Nano-composites and GaN Nanowires 28

3.1.2 Materials for PGaN 29

3.1.3 Materials for NH_3 Gas Sensor 29

3.2 Fabrication of GaN-Ga_2O_3 Nano-composites 29

3.3 Fabrication of GaN Nanowires 30

3.4 Fabrication of Porous GaN (PGaN) 35

3.5 Device Fabrication 36

3.5.1 GaN Nanowires Based NH_3 sensor 36

3.5.2 PGaN Based NH_3 Sensor 39

3.5.3 Testing of NH_3 Sensor 40

3.6 Characterizations 41

3.6.1 Field Emission Scanning Electron Microscope (FESEM) and Energy Dispersive X-rays (EDX) 41

3.6.2 Transmission Electron Microscope (TEM) 46

3.6.3 High Resolution X-ray Diffraction (HR-XRD) 47

3.6.4 Photoluminescence (PL) and Raman spectroscopy 51

3.7 Summary 54

CHAPTER 4 – RESULTS AND DISCUSSIONS

4.1 GaN-Ga_2O_3 Nanocomposites 55

4.1.1 Morphological Studies of GaN-Ga_2O_3 Nanocomposites 55

4.1.2 HR-XRD Analysis of the Nanocomposites 61

4.1.3 Raman Spectroscopy of the Nanocomposites 64

4.1.4 PL spectroscopy of the Nano-composites 66

4.2 Preliminary Studies of GaN Nanowires 68

4.2.1 Morphological studies of Nanowires 68

4.2.2 XRD Patterns of Curled GaN Nanowires 71

4.2.3 Growth Mechanism of Curled GaN Nanowires 74

4.2.4 PL Spectroscopy of Curled GaN Nanowires 79

4.2.5 Raman Spectroscopy of Curled GaN Nanowires 81

4.3 Preliminary Studies of GaN Nanowires on Different NH_3 Flow Rates.. 84

4.3.1 Surface Morphology of GaN Nanowires 84

4.3.2 HR-XRD of GaN Nanowires 87

4.3.3 Growth Mechanism of the GaN Nanowires 90

4.3.4 Raman Spectroscopy of GaN Nanowires 93

4.3.5 PL Spectroscopy of GaN Nanowires 97

4.4 Catalyst Dependent Studies on VLS Grown Nanowires 99

4.4.1 Morphological Aspects of Nanowires Grown from Various Catalysts 99

4.4.2 HR-XRD Analysis on GaN Nanowires 104

4.4.3 Characteristics of Fe Catalyst 108

4.4.4 Characteristics of Ni Catalyst 110

4.4.5 Characteristics of Au Catalyst 112

4.4.6 Proposed Growth Mechanism based on Fe Catalyst 113

4.4.7 Proposed Growth Mechanism based on Ni Catalyst 116

4.4.8 Proposed Growth Mechanism based on Au Catalyst 119

4.4.9 PL spectroscopy of GaN Nanowires.. 121

4.4.10 Raman Spectroscopy of GaN Nanowires 123

4.5 Characteristics of Temperature Dependent Nanowires Growth 125

4.5.1 Morphological Aspects of the Nanowires 125

4.5.2 Structural Studies of GaN Nanowires....................................... 129

4.5.3 EDX Measurements and Absorption/precipitation Behaviour .. 133

4.5.4 PL and Raman Spectroscopy of GaN Nanowires...................... 136

4.6 The Studies of Porous GaN 142

4.6.1 Surface Morphology of Porous GaN 142

4.6.2 Current-transient Profile and Growth Mechanics...................... 145

4.6.3 X-ray Diffraction Studies of Porous GaN 151

4.6.4 Raman Spectroscopy of Porous GaN 155

4.6.5 PL Spectroscopy of Porous GaN 157

4.7 Preliminary Studies of Prototype Nanostructured GaN-based NH_3 Sensor.. 160

4.7.1 Morphology of GaN Nanowires-based NH_3 Sensor.................. 160

4.7.2 Sensing Characteristics of GaN Nanowires-based NH_3 Sensor 161

4.7.3 Sensing Characterisatics of Porous GaN 169

4.8 Summary 173

CHAPTER 5 – CONCLUSIONS AND RECOMMENED FUTURE STUDIES

5.1 Conclusions 178

5.2 Recommended Future Studies 180

REFERENCES 182

APPENDIX A 196

LIST OF TABLES

PAGE

Table 2.1	Growth parameters and characteristics of GaN nanowires.	8-11
Table 3.1	Summaries of experimental conditions for GaN-Ga_2O_3 nano-composites and GaN nanowires.	34
Table 3.2	Anodization conditions for PGaN.	36
Table 3.3	Summarized experimental conditions for NH_3 sensor testing.	41
Table 4.1	List of peak positions, *d*-spacing, and lattice constants for the nanocomposite samples.	64
Table 4.2	XRD peak positions for both observed and reference samples.	74
Table 4.3	List of peak positions and calculated lattice constants.	88
Table 4.4	List of peak positions and calculated lattice constants.	108
Table 4.5	$t_{response}$ and $t_{recovery}$ of the sensor under different NH_3 flow rate.	169
Table 4.6	Summary of parameters for as-grown and PGaN based sensor.	170
Table 4.7	$t_{response}$ and $t_{recovery}$ of as-grown and PGaN.	172
Table A.1	The corresponding Ga (at%) at solidus and liquidus line for each catalyst	199

LIST OF FIGURES PAGE

Figure 2.1 VLS growth of Si nanowire, (a) absorption and formation of liquid Au-Si, (b) growth of Si nanowire. Adapted and redrawn from Wagner and Ellis (1964). 18

Figure 2.2 Electroless PEC setup. Adapted and redrawn from Youtsey *et al.* (1997). 23

Figure 3.1 (a) Digital photography of the thermal evaporator, (b) Schematic workings of vacuum thermal evaporation system. 31

Figure 3.2 (a) Digital image of the CVD system, (b) Schematic workings of the CVD system. 32

Figure 3.3 Electrochemical setup for PGaN fabrication. 35

Figure 3.4 Drawings of GaN nanowires based NH_3 sensor. 37

Figure 3.5 Workings of RF sputtering system. 38

Figure 3.6 Layouts of Porous GaN based NH_3 sensor. 39

Figure 3.7 Gas chamber used for NH_3 sensor testing. 40

Figure 3.8 FESEM and EDX system in NOR lab. 42

Figure 3.9 Matter-electron interactions, generation of (a) BSE, (b) SE, (c), x-rays (Hafner, 2007; Goldstein *et al.*, 2003). 44

Figure 3.10 Simple schematics of FESEM-EDX system. 45

Figure 3.11 Simple schematics of TEM (Reimer and Kohl, 2008). 47

Figure 3.12 HR-XRD system in NOR lab. 48

Figure 3.13 Illustration of Bragg's Law (Cullity, 1956). 49

Figure 3.14 Workings of HR-XRD at 2θ phase analysis (Cullity, 1956). 50

Figure 3.15 (a) PL and Raman system connected to optical microscope, (b) Drawings of PL-Raman system. 51

Figure 3.16 Radiative recombinations depicting PL mechanism. 52

Figure 3.17 Various types of light scattering. 53

Figure 4.1	FESEM images of (a) Ga_2O_3 powder, (b) MWCNTs.	56
Figure 4.2	FESEM images of (a) CP1-FR100, (b) CP1(CNT)-FR100 (the blue square indicates the region where nanowires observed), (c) nanowires as observed from (b).	57
Figure 4.3	Proposed formation mechanism of (a) CP1-FR100, (b) CP1(CNT)-FR100.	58
Figure 4.4	HR-XRD patterns of Ga_2O_3 and nanocomposites. The "X" peaks, although not indexed, however they were highly possible ascribed to Ga_2O_3.	62
Figure 4.5	Raman spectra of Ga_2O_3 and the nanocomposites.	65
Figure 4.6	PL spectra of GaN-Ga_2O_3 nanocomposites.	67
Figure 4.7	FESEM images of GaN nanowires at different magnifications, (a, b, c) OS1-FR70, (d, e, f) OS1-FR70-Si.	69
Figure 4.8	TEM images of GaN nanowires at different magnifications, (a, b) OS1 FR70, (c, d) OS1-FR70-Si. The region between yellow lines indicates possible defects zone.	69
Figure 4.9	Histogram about size distribution of GaN nanowires with fitted Gaussian profile (indicated as dashed lines).	70
Figure 4.10	XRD patterns of grown GaN nanowires.	72
Figure 4.11	Proposed growth mechanism of curled GaN nanowires. Fe_2N was omitted from this drawing.	75
Figure 4.12	PL spectra of GaN nanowires. The dashed lines indicate the deconvoluted components of the broad luminescence band.	80
Figure 4.13	Raman spectra of GaN nanowires.	82
Figure 4.14	FESEM micrographs of sample (a) EFC1-FR50, (b) EFC1-FR100, (c) EFC1-FR150. (d). TEM micrograph from sample EFC1-FR50.	85
Figure 4.15	(a-c) Gaussian fitted histograms for GaN nanowires size distribution. (d) Plot of mean nanowires size (both high and low frequency counts) against NH_3 flow rates.	87
Figure 4.16	HR-XRD patterns of GaN nanowires. The intensities between 50~80˚ are magnified by ten times, indicated as "× 10" in the figure.	88

Figure 4.17	Proposed growth mechanism of HAR- and Lr-GaN nanowires. The platforms that held either catalyst of nanowires/rods are *c*-plane sapphire.	91
Figure 4.18	Raman spectra of GaN nanowires. The deconvoluted components were indicated as dashed blue lines.	94
Figure 4.19	Relative intensity ratios of E_2(high)/A_1(LO) and AOT/E_2(high) against NH_3 flow rate.	96
Figure 4.20	PL spectra of GaN nanowires. The deconvoluted components were indicated as dashed blue lines.	97
Figure 4.21	Electron micrographs of GaN nanowires grown using Fe catalyst. (a) and (b) from FESEM, while (c) from TEM.	100
Figure 4.22	Electron micrographs of GaN nanowires grown using Ni catalyst. (a-d) from FESEM, (e, f) from TEM. (d) and (f) represented magnified view from circled region of (c) and (e) respectively.	101
Figure 4.23	Electron micrographs of GaN nanowires grown using Au catalyst. (a-d) from FESEM, (e, f) from TEM. (d) and (f) represented magnified view from circled region of (c) and (e) respectively.	103
Figure 4.24	Histogram plots of GaN nanowires size distribution based on (a) Fe, (b) Ni, and (c) Au catalyst.	104
Figure 4.25	(a) XRD patterns of GaN nanowires; the regions between 50~80˚ have been magnified as indicated, (b) Ni-Ga phases, (c) magnified view for GC1-FR250 to show the presence of Au.	106
Figure 4.26	Proposed growth mechanism of Fe-catalyst based GaN nanowires. (a) highly localized growth, (b) coalesced and slow growth, and (c) typical and moderate growth as seen in most Fe-catalyst based samples.	114
Figure 4.27	Proposed growth mechanism of Ni-catalyst based GaN nanowires.	118
Figure 4.28	Proposed growth mechanism of Au-catalyst based GaN nanowires.	120
Figure 4.29	PL spectra of GaN nanowires. The blue dash lines represented the deconvoluted bands.	122
Figure 4.30	Raman spectra of GaN nanowires. The blue dash lines represented the deconvoluted bands.	124

Figure 4.31	Micrographs of GaN nanowires grown using Fe catalyst at (a) 900˚C, (b) 950˚C, and (c) 1000˚C.	126
Figure 4.32	Micrographs of GaN nanowires grown using Ni catalyst at (a) 900˚C, (b) 950˚C, and (c) 1000˚C.	127
Figure 4.33	Micrographs of GaN nanowires grown using Au catalyst at (a) 900˚C, (b) 950˚C, and (c) 1000˚C.	127
Figure 4.34	Mean GaN nanowires size against growth temperatures.	128
Figure 4.35	XRD patterns of GaN nanowires grown using Fe-catalyst at different growth temperature.	130
Figure 4.36	XRD patterns of (a) GaN nanowires grown using Ni-catalyst, (b) Ni-Ga alloy at different growth temperature.	131
Figure 4.37	XRD patterns of GaN nanowires grown using Au-catalyst at different growth temperature.	132
Figure 4.38	Plot of EDX ratios of various catalysts against growth temperature.	134
Figure 4.39	PL spectra of GaN nanowires.	137
Figure 4.40	Raman spectra of GaN nanowires.	138
Figure 4.41	Electron Micrographs of the anodized GaN samples at various durations, (a) as-grown, (b) 5, (c) 10, (d) 20, (e) 40, and (f) 80 min, (g, h, i) represents magnified versions of (d, e, f) respectively. Encapsulated in the blue circles are nanopebbles.	143
Figure 4.42	Cross-section micrographs of anodized GaN samples at various durations, (a) 5, (b) 10, (c) 20, (d) 40, and (e) 80 min. Scale bar from (a) to (e) is valued 500nm.	145
Figure 4.43	Current-transient profiles for all anodized GaN. The texts inside each region signified the summary of insights obtained from it. The rectangle would be explained in text.	147
Figure 4.44	Schematic representation of pore formation mechanism, which began from (a) to (f).	149
Figure 4.45	(a) HR-XRD patterns of as-grown and PGaN samples and (b) sapphire reflections. $K_{\alpha 1}$ and $K_{\alpha 2}$ reflections of (004) GaN and (006) sapphire were clearly seen.	152
Figure 4.46	Plot of σ_a against anodization durations. The dashed line illustrated the trend of the data points.	154

Figure 4.47	Raman spectra for all samples.	156
Figure 4.48	PL spectra for all samples. The actual intensity is shown as the numerical figures next to the each spectrum.	158
Figure 4.49	Micrographs of Pd-functionalized GaN nanowires viewed from, (a, b) SE, (c, d) BSE mode. The decorated particles on the nanowires surface were Pd, shown with higher contrast in (c,d).	161
Figure 4.50	I-V characteristics of nanowires-based NH_3 sensor operate at (a) air, (b) NH_3 ambient.	163
Figure 4.51	Plot of sensitivity against sensing temperature.	164
Figure 4.52	Plot of $\Delta\Phi_B$ against sensing temperature.	166
Figure 4.53	I-t profiles of nanowires based NH_3 sensors on different NH_3 flow.	168
Figure 4.54	I-V characteristics of PGaN based NH_3 sensor.	170
Figure 4.55	I-t profiles of as-grown and PGaN based NH_3 sensor.	171
Figure A.1	Binary phase diagram for Fe-Ga system (Okamoto, 1990).	197
Figure A.2	Binary phase diagram for Ni-Ga system (Okamoto, 2008).	198
Figure A.3	Binary phase diagram for Au-Ga system (Elliot and Shunk, 1981).	199

LIST OF ABBREVIATIONS

1D	one dimensional
2D	two dimensional
3D	three dimensional
AOT	acoustic overtone
atm	atmospheric
BL	blue luminescence
BSE	back scattered electrons
CBM	conduction band minimum
CNTs	carbon nanotubes
CVD	chemical vapour deposition
DI	deionized
e-beam	electron beam
EDX	energy dispersive x-rays
FET	field effect transistor
FWHM	full-width at half-maximum
HAR-	high aspect ratio
HRTEM	high-resolution transmission electron microscope
HVPE	hydride vapour phase epitaxy
ICDD-PDF	International Center of Diffraction Data-Powder Diffraction File
ICP-RIE	inductive coupled-reactive ion etching
IPA	isopropyl alcohol
I-t	current-time
I-V	current-voltage
LCG	laser-assisted catalytic growth

LED	light emitting diode
LO	longitudinal optical
Lr-	larger (to descirbed nanowires only)
MBE	molecular beam epitaxy
MWCNTs	multi-walled carbon nanotubes
NBE	near band emission
N-H	nitrogen-hydrogen
PEC	photoelectrochemical
PGaN	porous GaN
PL	photoluminescence
QMS	quadrupole mass spectrometry
Ref.	References
RF	radio frequency
RHEED	reflection high energy electron diffraction
RIR	relative intensity ratio
RL	red luminescence
sccm	standard cubic centimeter per minute
SE	secondary electrons
SMU	source measuring unit
SO	surface optical
TEM	transmission electron microscope
TMGa	trimethylgallium
TO	transverse optical
UV	ultra-violet
UVL	ultra-violet luminescence

V	voltage (unit for voltage)
VBM	valence band maximum
v/v	volume-to-volume
V_{Ga}	gallium vacancy
$V_{Ga}O_N$	gallium vacancy-oxygen substitute nitrogen
VLS	vapour-liquid-solid
VPE	vapour phase epitaxy
VS	vapour-solid
VSS	vapour-solid-solid
XRD	x-ray diffractions
ZBP	zone-boundary phonon

LIST OF SYMBOLS

Symbol	Description
(hkl)	Miller indices (dimensionless)
2θ	Diffraction angle from XRD (measured in degree)
A	area of the metal contact (measured in cm^2)
a	lattice constant (measured in nm)
A^*	Richardson constant (measured in A $cm^{-2}K^{-2}$)
a_0	lattice constant a for bulk GaN (measured in nm)
a_p	lattice constant a for PGaN (measured in nm)
c	lattice constant (measured in nm)
c_0	lattice constant c for bulk GaN (measured in nm)
C_{ij}	elastic constant (measured in GPa), i and j = integer
c_p	lattice constant c for PGaN (measured in nm)
$K_{\alpha 1}$	k-alpha 1 radiation (measured in nm)
$K_{\alpha 2}$	k-alpha 2 radiation (measured in nm)
d	interatomic spacing (measured in nm)
$\Delta\Phi_B$	difference in Schottky Barrier Height (measured in meV)
d_{hkl}	interatomic spacing corresponded to *(hkl)*
e^-	Electrons
e^{-1}	inverse of exponential
ε_a	biaxial strain (dimensionless)
ε_c	Strain (dimensionless)
Φ_B	Schottky Barrier Height (measured in eV)
$\Phi_{B(air)}$	Schottky Barrier Height (air ambient) (measured in eV)

$\Phi_{B(NH_3)}$	Schottky Barrier Height (NH_3 ambient) (measured in eV)
$I_{air\ ambient}$	current measured under NH_3 ambient (measured in mA)
$I_{NH_3\ ambient}$	current measured under NH_3 ambient (measured in mA)
I_{peak}	peak current (measured in mA)
I_S	saturation current (measured in mA)
$I_{S(air)}$	saturation current under air ambient (measured in mA)
$I_{s(NH_3)}$	saturation current under NH_3 ambient (measured in mA)
k	Boltzmann constant (measured in eV K^{-1})
q	electronic charge (eV)
$\boldsymbol{q}$	wavevector
θ_{hkl}	diffraction angle corresponded to *(hkl)*
σ_a	biaxial stress (measured in GPa)
S_F	Sensitivity (dimensionless, converted to percentage by multiplying with 100.
sin θ	sin theta (dimensionless)
T	absolute temperature (measured in Kelvin)
$t_{recovery}$	recovery time (measured in seconds)
$t_{response}$	response time (measured in seconds)
λ	x-rays wavelength (measured in nm)

LIST OF PUBLICATIONS

Beh, K. P., Yam, F. K., Chin, C. W., Tneh, S. S. and Hassan, Z. (2010). The growth of III–V nitrides heterostructure on Si substrate by plasma-assisted molecular beam epitaxy, *Journal of Alloys and Compounds* **506**: 343-346.

Beh, K. P., Yam, F. K., Low, L. L. and Hassan, Z. (2013). One-step growth of curled GaN nanowires using chemical vapor deposition method, *Vacuum* **95**: 6-11.

Beh, K. P., Yam, F. K., Low, L. L., Tneh, S. S., Ng, S. W., Tan, L. K., Chai, Y. Q. and Hassan, Z. (2012). Growth and investigations of GaN-Ga_2O_3 nano-composites, *Optoelectronics and Advanced Materials - Rapid Communications* **6**: 1015-1018.

Beh, K. P., Yam, F. K., Tan, L. K., Ng, S. W., Chin, C. W. and Hassan, Z. (2013). Photoelectrochemical Fabrication of Porous GaN and Their Applications in Ultraviolet and Ammonia Sensing, *Japanese Journal of Applied Physics* **52**: 08JK03.

Beh, K. P., Yam, F. K., Tneh, S. S. and Hassan, Z. (2011). Fabrication of titanium dioxide nanofibers via anodic oxidation, *Applied Surface Science* **257**: 4706-4708.

Chai, Y., Tam, C. W., Beh, K. P., Yam, F. K. and Hassan, Z. (2013). Porous WO_3 formed by anodization in oxalic acid, *Journal of Porous Materials* **20**: 997-1002.

Chin, C. W., Yam, F. K., Beh, K. P., Hassan, Z., Ahmad, M. A., Yusof, Y. and Bakhori, S. K. M. (2011). The growth of heavily Mg-doped GaN thin film on Si substrate by molecular beam epitaxy, *Thin Solid Films* **520**: 756-760.

Low, L. L., Yam, F. K., Beh, K. P. and Hassan, Z. (2011). The influence of Ga source and substrate position on the growth of low dimensional GaN wires by chemical vapour deposition, *Applied Surface Science* **257**: 10052-10055.

Low, L. L., Yam, F. K., Beh, K. P. and Hassan, Z. (2011). The influence of growth temperatures on the characteristics of GaN nanowires, *Applied Surface Science* **258**: 542-546.

Ng, S. W., Yam, F. K., Beh, K. P. and Hassan, Z. (2014). Titanium Dioxide Nanotubes in Chloride Based Electrolyte: An Alternative to Fluoride Based Electrolyte, *Sains Malaysiana* **43**: 947-951.

Ng, S. W., Yam, F. K., Beh, K. P., Theh, S. S. and Hassan, Z. (2011). The effect of growth parameters and mechanism of titania nanotubes prepared by anodic process, *Optoelectronics and Advanced Materials - Rapid Communications* **5**: 258-262.

Ng, S. W., Yam, F. K., Low, L. L., Beh, K. P., Mustapha, M. F., Sota, E. N., Tneh, S. S. and Hassan, Z. (2011). Self-assembled ZnO nanostripes prepared by acidified ethanolic anodization, *Optoelectronics and Advanced Materials - Rapid Communications* **5**: 89-91.

Tan, L. K., Yam, F. K., Beh, K. P. and Hassan, Z. (2013). Study of growth mechanism of self-catalytic branched GaN nanowires, *Superlattices and Microstructures* **58**: 38-43.

Tan, L. K., Yam, F. K., Low, L. L., Beh, K. P. and Hassan, Z. (2014). The influence of growth temperatures on the characteristics of GaN nanowires: The Raman study, *Physica B: Condensed Matter* **434**: 101-105.

Tneh, S. S., Hassan, Z., Saw, K. G., Yam, F. K., Beh, K. P. and Abu Hassan, H. (2010). Investigation of non-annealed Al ohmic contacts on undoped ZnO synthesized using the "bottom-up" growth method, *Optoelectronics and Advanced Materials - Rapid Communications* **4**: 965-967.

Yam, F. K., Beh, K. P., Ng, S. W. and Hassan, Z. (2011). The effects of morphological changes on the vibrational properties of self-organized TiO_2 nanotubes, *Thin Solid Films* **520**: 807-812.

Abdullah, N., Yam, F. K., Beh, K. P., Abdullah, Q. N. and Hassan, Z. Study of Indium Oxide materials grown at different temperatures. *Regional Annual Fundamental Science Symposium (RAFSS)*, Persada Johor International Convention Centre, Johor Bahru, Malaysia.

Beh, K. P., Yam, F. K., Low, L. L. and Hassan, Z. Structural Studies of GaN-nanowires Grown at Different Ammonia Flow Rate. *Asian International Conference on Materials, Minerals and Polymer (MAMIP)*, Vistana Hotel, Penang, Malaysia.

Beh, K. P., Yam, F. K., Shahrudin, S., Ahmad Bislaman, S. N. S. and Hassan, Z. GaN Nanowires and Nanoribbons: Effects of Ammonia Flow Rate on Structural and Vibrational Properties. *4th International Conference On Solid State Science And Technology (ICSSST)*, Holiday Inn Melaka, Melaka, Malaysia.

Tan, L. K., Yam, F. K., Beh, K. P. and Hassan, Z. The Investigation of Morphological Characteristics of Porous Anodic Alumina Generated by Electrochemical Etching. *Asian International Conference on Materials, Minerals and Polymer (MAMIP)*, Vistana Hotel, Penang, Malaysia.

FABRIKASI DAN KAJIAN NANO-STRUKTUR GaN DAN APLIKASI DALAM PENGESANAN GAS AMMONIA

ABSTRAK

Dalam kerja ini, nanodawai GaN, GaN berliang (PGaN), dan pengesan gas ammonia (NH_3) telah difabrikasi dan dikaji. Sampel nanodawai GaN dalam kerja ini ditumbuh dengan kaedah pemendapan wap kimia (CVD), yang bermod pertumbuhan wap-cecair-pepejal (VLS). Untuk pengajian nanodawai GaN, tumpuan diberi terhadap mekanisma pertumbuhan VLS, terutamanya kesan pemangkin logam. Sebelum itu, beberapa parameter pertumbuhan yang sesuai untuk system CVD perlu ditentukan. Kerja ini terdiri daripada kesan pengnitridaan Ga_2O_3, substrat penumbuhan (Si dan nilam bersatah-*c*), dan pengaliran optimum NH_3. Dari kerja yang dinyatakan, Ga_2O_3 dan nilam bersatah-*c* telah dipilih sebagai prakursor dan substrat masing-masing, manakala pengaliran NH_3 telah diset sebanyak 250 sccm bagi kerja seterusnya. Dari kajian tentang kesan pemangkin terhadap pertumbuhan nandawai GaN, keadaan tepu pemangkin logam disimpul dengan menggunakan keputusan pembelauan sinar-x (XRD) bersama gambarajah fasa. Didapati bahawa bagi besi (Fe), ia berada pada Fe_6Ga_5, dengan fasa campuran pepejal-cecair. Walau bagaimanpun, komponen cecair berkurang dengan suhu, dan menjadi pepejal sepenuhnya pada 900˚C. Pealihan fasa depercayai menggalakkan penumbuhan permukaan (*h*00), justeru menyebabkan nanodawai bengkok. Bagi nickel (Ni), aloinya kekal pada keadaan pepejal sepenuhnya, manakala Ni_5Ga_3 dipercayai sebagai keadaan tepu. Menariknya, Ni-Ga boleh tepu berlebihan, mengakibatkan pembentukan reben-nano pada 1000˚C. Keadaan tepu emas (Au) sukar ditentukan, sejak sedikit galium (Ga) (<1 at%)

mencukupi untuk menepukan Au. Tambahan pula dengan keadaan penumbuhan, nanodawai mempunyai morfologi yang unik dan nenunjukan penumbuhan berorientasi-*c*. Dari segi fizikal, diameter nanodawai bagi pemangkin Ni antara 60 hingga 80 nm; manakala Fe 100 hingga 160 nm. Pemangkin Au menghasilkan nanodawai bersaiz besar, antara 140 hingga 200 nm. Keputusan foto pendarcahaya (PL) mencadangkan kewujudan tegasan antara muka dan gangguan permukaan, manakala jalur Raman peringkat pertama dibawah petua pilihan menunjukan nanodawai GaN yang berstruktur wurtzit heksagon, bersama dengan mod tambahan yang disebabkan oleh kesan nanosaiz dari nanodawai. kehadiran GaN, bersama dengan ciri-ciri nanodawai. PGaN telah dihasilkan dengan teknik foto penganodan, dengan masa sebagai pembolehuhbah. Morfologi berliang telah diperolehi dan penganodan berlebihan boleh mengakibatkan pemecahan filem GaN. Oleh demikian, satu mekanisma telah dicadangkan. Keputusan XRD dan PL menunjukan penurunan dari segi tekanan dwipaksi pada sampel berliang. Adalah didapati bahawa purata individu luas liang bagi sampel dianodakan dalam 5, 10, dan 20 minit adalah di sekitar 1566, 2575, and 2885 nm^2 masing-masing. Sementara itu, dua prototaip pengesan NH_3 telah dibuat da didapati mempunyai ciri-ciri diod. Yang berdasarkan nanodawai GaN menunjukan kepekaan bertingkat dengan suhu, manakala bandingan antara filem GaN dan PGaN menunjukan yang kedua lebih peka dalam pengesanan. Mekanisma pengesanan adalah sama bagi kedua-dua sampel, berdasarkan perubahan antara kepekatan NH_3 dengan oksigen (O_2). Bagi sample nanodawai GaN, kepekaan (S_F) (pada 3V, 350°C) adalah 109% dengan purata masa respons dan pemulihan ($t_{response}$, $t_{recovery}$) kira-kira 10 dan 2s masing-masing. Di samping itu, S_F (pada 5V, 350°C) bagi filem GaN (PGaN) adalah 48.2% (26.1%), manakala $t_{response}$ and $t_{recovery}$ kira-kira 17s (35.3s) dan 19.2s (8.2s) masing-masing.

FABRICATION AND INVESTIGATION OF GaN NANOSTRUCTURES AND THEIR APPLICATIONS IN AMMONIA GAS SENSING

ABSTRACT

In this work, gallium nitride (GaN) nanowires, porous GaN (PGaN), and ammonia (NH_3) gas sensors have been fabricated and studied. The GaN nanowires samples in this work were grown using chemical vapour deposition (CVD) method, additionally employing vapour-liquid-solid (VLS) growth mode. For the studies of GaN nanowires, VLS growth mechanism, particularly the effects of metal catalyst was focused upon. Prior to that, several growth parameters that suits the CVD system have to be determined first. This comprised of several works, which were nitridation effects towards gallium (III) oxide (Ga_2O_3), growth substrates [silicon (Si) and *c*-plane sapphire], and optimum NH_3 flow rate. From the aforementioned works, Ga_2O_3 and *c*-plane sapphire have been chosen as the precursor and substrate respectively, while NH_3 flow rate was set to 250 standard cubic centimeter per minute (sccm) in the subsequent works. From the studies of catalyst effects towards GaN nanowires growth, the saturation state of metal catalyst could be deduced using x-ray diffraction (XRD) results along with available phase diagrams. It was revealed that iron (Fe) saturated around Fe_6Ga_5, under solid-liquid mixture state. However, the liquid content of the alloy decreases with temperature, subsequently become solid at 900˚C. The state transitions were believed to promote the growth of (h00) facets thus resulted in curled and bended nanowires. For nickel (Ni), the alloy remained solid entirely, while Ni_5Ga_3 was believed to be the saturation state. Interestingly, Ni-Ga could be oversaturated, resulted in the formation of nanoribbons as seen at

1000˚C. The saturation state of gold (Au) was difficult to determine, since very little amount of gallium (Ga) (< 1 at%) sufficient to saturate it. Coupled with the growth conditions, the resulting nanowires have a unique morphology that strongly suggested *c*-oriented growth. On the physical characteristics, the nanowires diameter for Ni catalyst ranging from 60 to 80 nm; while that of Fe catalyst 100 to 160 nm. Au catalyst produced nanowires of greatest size (diameter), ranging from 140 to 200 nm. Photoluminescence (PL) results suggested the presence of interfacial stress and surface disorder, while the first order Raman bands under Selection rule revealed the GaN nanowires to be hexagonal wurtzite structure, along with additional modes due to nanosize effects from the nanowires. PGaN was produced by photo-enhanced anodization technique with duration as variable. Porous morphology had been obtained and prolonged anodization resulted in breakdown. A growth mechanism has been proposed for that. It was found that the average individual pore area of sample anodized for 5, 10, and 20 minutes was about 1566, 2575, and 2885 nm^2 respectively. The XRD and PL results showed relaxation of biaxial compressive stress in porous samples. Meanwhile, two prototype NH_3 gas sensors were made and have a rectifying behaviour. On that of GaN nanowires exhibited increased sensitivity with working temperature, while comparison between as-grown and PGaN showed the latter being superior in sensing. The sensing mechanism was similar in both samples, where based on the changes between NH_3 and oxygen (O_2) concentrations. For GaN nanowires sample, the sensitivity (S_F) (at 3V, 350°C) was 109% with average response and recovery time ($t_{response}$, $t_{recovery}$) about 10 and 2s respectively. Meanwhile, S_F (at 5V, 350°C) of as-grown (PGaN) was 48.2% (26.1%), while that of $t_{response}$ and $t_{recovery}$ about 17s (35.3s) and 19.2s (8.2s) respectively.

CHAPTER 1

INTRODUCTION

1.1 The Background of Gallium Nitride

Gallium Nitride (GaN) is a well-known semiconductor material that often associated with device applications, particularly in the optoelectronics field. With a wide band gap about 3.4 eV [corresponded to the ultra-violet (UV) wavelength of 365 nm] at 300 K, it was ascertained that GaN would be a suitable candidate for fabricating UV-based optoelectronics, such as light emitting diode (LED) and photodetector (Chang et al., 2010, Yoon et al., 2010). Aside from that, GaN is both thermally and chemically stable, thus has been used in fabricating high performance devices such as field effect transistor (FET) that operates on harsh environments (Pearton et al., 1999, Li and Waag, 2012).

To date, GaN takes the form of either thin film or nanostructures. Prior to the dawn of nanotechnology, research and development have been primarily focused upon the former and still ongoing. As a result, many GaN based devices were derived from thin film technology. In recent years, more attentions have been heeded towards nanostructured GaN. Due to their unique properties such as larger surface areas and lower level of defects (compared to thin film), they are more suitable to be building blocks for highly sensitive and greater performance devices. Since then, many works have been conducted and contributed to literature.

1.2 Nanostructured GaN and NH_3 Gas Sensing

Many kinds of GaN based nanostructures have been reported in literature such as nanodots, nanowires, and nanoporous. Among them, nanowires and porous GAN (PGaN) played a vital role in the research and development of nitride based technology.

In many years of GaN studies, the fabrication of GaN nanowires was first reported by Han (1997), who demonstrated such growth using carbon nanotubes as templates. Due to the absence of planar substrates, powdered products were obtained. Wafer scale GaN nanowires was inspired by Cheng et al. (1999), who utilized anodic alumina mask with vertical pore channels to confine the reactants as to induce growth. Since then, many growth variations have been introduced.

The growth of GaN nanowires using chemical vapour deposition (CVD) method remains a popular choice to date owing to the simplicity and flexibility of both growth apparatus designs and control parameters. In general, each CVD reactor is uniquely tailored based on user preferences. As a result, the reported growth parameters often differed from each other (Stern et al., 2005, Djurišić et al., 2007). In this work, effects of ammonia (NH_3) flow rates, temperature, metal catalyst, and substrates would be studied upon.

Metal catalyst such as gold (Au) and nickel (Ni) often used to assist the growth of nanowires through vapour-liquid-solid (VLS) mechanism. In general, the mechanism could be simplified as follows: The catalyst firstly forms an alloy with the vapour phase reactants (Ga and N species) through absorption, while upon reaching saturation, GaN nanowires would precipitate out from it (Rao et al., 2003, Qin et al., 2008, Chèze et al., 2010). The accompanied assumption that frequently made was the catalyst undergone liquefaction during alloying, resulting in coalescence among neighbour to form bigger droplets, which lead to nanowires of greater diameter.

However, this has been shown otherwise, for example, Ni, remained solid throughout nanowires growth (Chèze et al., 2010). Such feature is of importance and could be exploited in tailoring the size of the nanowires during growth. However, literature about the aforementioned are scarce.

There are many variation of precursors for GaN. The N-component usually contributed by NH_3, which is in gaseous state. For Ga-component, solid precursors such as gallium (Ga) metal or gallium (III) oxide (Ga_2O_3) powder, and gaseous, trimethylgallium (for MOCVD) have been used. Many works have been reported the use of Ga_2O_3 powder as a potential precursor. In order for Ga_2O_3 to become GaN, the former would be heated above 900°C (also the growth temperature of GaN) and reacted with streams of NH_3. This process is known as nitridation. The N-component of NH_3 would diffuse into Ga_2O_3, displacing and substituting O concurrently. This process was further sped up with the introduction of hydrogen (H_2), derived from dissociated NH_3. H_2 would leach out O from Ga_2O_3, forming H_2O that subsequently exit through the exhaust.

PGaN is essential in both GaN nano- and thin film technology. Typical PGaN can be fabricated using PEC method. The nanoporous morphology significantly increased the surface area of PGaN, which suitable for higher sensitivity device to be made. Interestingly, areas with defects such as threading dislocation was removed via etching. With subsequent deposition of epilayer, a more relaxed layer could be obtained.

GaN usually found in optoelectronics applications. Aside from that, gas sensing applications have been investigated as well. In general, gas sensing could be achieved when the semiconductor material is heated at elevated temperature. In case

of NH_3, both heat and corrosive environment would be present. The thermal and chemical stability of GaN thus makes it suitable candidate for NH_3 gas sensors.

1.3 Research Goals and Novelties

The studies of GaN nanowires here primarily focused upon the VLS growth mechanism, particularly the effects of catalyst towards the characteristics of the grown nanowires. As mentioned previously, the state of the catalyst could affect the physical aspects of the nanowires. Here, other characteristics such as structural and vibrational properties would be investigated as well. For that, catalyst with state of solid, liquid, and mixture of both during saturation phase are required. Au, Ni, and iron (Fe) have been chosen since the amount of Ga for liquefaction differs from each other. Details about liquefaction can be obtained from their respective phase diagrams (see Appendix 1). It should be noted that the aforementioned liquefaction was used as a reference point, while the catalyst need not necessary to liquefy to trigger nanowires growth.

Direct determination of the catalyst state on saturation phase would be difficult to probe. Fortunately, as each catalyst at saturation would have a unique alloy phase (as referenced from phase diagrams), they could be detected post-growth using XRD. Hence, the experimental work has been slightly modified relative to those reported in literature, i.e. depositing thicker layer of catalyst. This would allow more signals to be contributed by the alloy phase. (To our best of knowledge such technique is rarely used).

In order to achieve the aforementioned goal, few preliminary works have to be done for determining a suitable set of growth parameters for the self-assembled CVD system. The first work focuses upon the suitability of Ga_2O_3 being a Ga-precursor for GaN nanowires, which could be determined through nitridation process. The next

work would be identifying suitable substrates for GaN nanowires growth. The effects of Si and c-plane sapphire towards GaN nanowires growth are investigated. The subsequent work emphasizes about the flow rate of NH_3, since this is essential in ensuring continuous growth of GaN nanowires without unexpected hindrance.

The studies of PGaN had remained an interesting topic to date. Although it could be obtained through many methods, photo-enhanced anodization would be primarily focused upon in this work. Despite the method's simplicity, having control and maintaining over the porous morphology remained a challenging task. Hence, in this work, it is essential to investigate the pore formation to destruction mechanism chronologically. Concurrently, the characteristics of PGaN would be studied as well.

Utilizing GaN based nanostructures in device fabrications remained topic of interest, given their unique features and advantages. In this work, integration of GaN nanowires and PGaN towards ammonia (NH_3) gas sensing purposes would be attempted. In order to evaluate the response of the nanometerials towards that, simplicity in sensor designs is highly desired. Additionally, it was believed that the obtained results could prove to be useful when developing intricate sensors, which would become a standalone field of research.

1.4 Organization of Thesis Chapters

This thesis is divided into five main chapters. Chapter one briefly introduced the general aspects of GaN and their applications, subsequently followed by that of GaN nanowires and PGaN. The aims and objectives about the thesis work would be stated and cursory elucidated. Finally, general introduction of each chapter was covered as well.

Chapter two mainly covers on literature reviews about the growth aspects and characteristics of GaN nanowires. Aiding to the discussion would be a summary table about the growth properties done found in literature. Next, brief introduction about the early works on PGaN will be provided. The topics on NH_3 and related gas sensors would be included as well.

Chapter three is related to methodologies. There, the materials and technique used in fabricating GaN nanostructures would be elaborated. In addition, this chapter also provides introductory discussions on the growth apparatus as well as characterization tools used in this work.

Chapter four heavily emphasizes on the obtained results and discussions, and. is further divided into eight sections. The first three sections investigates suitable GaN nanowires growth parameters of the CVD system, which consisted of nitridation properties of GaN precursor, i.e. Ga_2O_3, substrates (Si and *c*-plane sapphire), and NH_3 flow rate. Next, the fourth section discusses about the aspects of GaN nanowires grown using different catalyst, which were Fe, Ni, and Au. The aforementioned results were further investigated by varying the growth temperature, as discussed under the fifth section. Then, PGaN, which is another form of GaN fabricated using different methods, is introduced as the sixth section. After that, the seventh section elucidates the NH_3 sensing characteristics of GaN nanowires and PGaN. The summary of chapter four is provided in the eighth section.

Finally, chapter five concludes the thesis work so far, as well as proposes possible future works in light of improving the current research.

CHAPTER 2

LITERATURE REVIEW

In this chapter, literature studies about the growth and characteristics of GaN nanowires and PGaN would be reviewed. In additional, a brief topic about NH_3 gas sensors was included. Although some topics might be too wide to be covered, those related to the works presented in this thesis were covered instead.

2.1 Introductions to GaN Nanowires

In many years of GaN based technology, the fabrication of GaN nanowires was first reported by Han (1997) (although the title of corresponding article used "GaN Nanorods", the authors credited the term "nanowires" in the contents). During that time, carbon nanotubes were used as templates to confine the vapour-state reactants for GaN nanowires production. Similar work was conducted by Zhu and Fan (1999), with the aid of transmission electron microscope (TEM) for better characterizations. Later on, Cheng et al. (1999) succeeded in fabricating nanowires in large-scale using anodic alumina mask with vertical pore channels, while the growth process was done using CVD method. Since then, many growth variations have been introduced. In light of that, the possible growth parameters in which could affect the overall fabrication process had been tabulated in Table 2.1.

Table 2.1: Growth parameters and characteristics of GaN nanowires.

References (Ref.)	Precursors				Substrate	Growth method	Growth ambient		Growth duration (min)	Size		Remarks
	Catalyst	Ga-source	N-source (flow)	Supporting (flow)			Pressure (Torr)	Temperature (˚C)		diameter (nm)	length (μm)	
(Han, 1997, Zhu and Fan, 1999)	(none)	Ga-Ga_2O_3 mixture	NH_3 (400)	-	CNTs (as template)	-	-	900	60	14.9	-	Diamater of CNT < 15 nm.
(Cheng et al., 1999)	(none)	Ga-Ga_2O_3 mixture	NH_3 (300)	-	porous alumina	-	-	1000	120	14	hundreds of μm	-
(Duan and Leiber, 2000)	Fe, Au	GaN	NH_3 (80)	-	quartz tube	laser-assisted catalytic growth (LCG)	250	900	5	10	> 1	(i). Growth observed on Fe, but not Au. (ii). Nanowires removed from quartz tube.
(Fan et al., 2001)	Fe	Ga-Ga_2O_3 mixture	NH_3 (100)	-	Si	CVD	-	900	10	60	-	Patterned Fe on substrate.
(Zhang and Zhang, 2002)	In	Ga	NH_3 (400)	-	porous alumina	-	vacuum	1000	120	20	> 20	-
(Seryogin et al., 2005)	Ni/Au	Ga	NH_3 (50~200)	HCl (1~10) (to react with Ga) N_2 (as carrier gas, 3000)	Si (111), *c*-plane sapphire	HVPE	-	800~850: precursor; 650~750: substrate	1~5	200~400	-	Au coated on Ni to serve as protective layer.

Table 2.1: (Continued)

Ref.	Precursors				Substrate	Growth method	Growth ambient		Growth duration (min)	Size		Remarks
	Catalyst	Ga-source	N-source (flow)	Supporting (flow)			Pressure (Torr)	Temperature (˚C)		diameter (nm)	length (μm)	
(Stern et al., 2005)	Ni, Fe	Ga-Ga_2O_3 mixture, Ga, Ga_2O_3	NH_3 (5~150)	-	alumina, SiO_2/Si	CVD	300, 760	850~1100	-	60~130	-	-
(Zhang et al., 2006)	Au	Ga-Ga_2O_3 mixture	NH_3 (200)	-	Si (001)	CVD	80	1000	200	100	several	Author proclaimed not VLS growth.
(Li et al., 2006)	(none)	Ga	NH_3 (50)	-	quartz	Nitridation , vapour transport	20	830, 1000	60~120	15~40	100	-
(Cai et al., 2006)	(none), Au, Ni, $Ni(NO_3)_2$	Ga	NH_3	Ar (different NH_3/Ar flow ratio)	Si (100), Si (111)	CVD	~3.5 (~465 Pa)	800, 850, 900, 950, 1000	30	too many to be listed		(i). SiO_x nanowires detected. (ii). Nanowires appeared from 950˚C onwards.
(Ji et al., 2007)	Ni	TMGa (3)	NH_3 (100)	H_2 as carrier gas, total flow rate = 400	*c*-plane sapphire	MOCVD	100	800, 900	10~20	150~300	5~10	-
(Lei et al., 2008)	(none)	Ga	NH_3 (30)	-	SiO_2	CVD	-	820	60	80	-	Zigzagged nanowires.
(Shin et al., 2008)	Ni	Ga_2O_3+ graphite	NH_3 (200~600)	Ar (2000~2500)	*c*-plane sapphire	VPE (similar to CVD)	760	1000~ 1100	90	60~120	-	-
(Qin et al., 2008b)	Co	Ga_2O_3	NH_3 (500 sccm)	-	Si (111)	nitridation process	-	900, 950, 1000	15	100~500	tens of μm	-

Table 2.1: (Continued)

Ref.	Precursors				Substrate	Growth method	Growth ambient		Growth duration (min)	Size		Remarks
	Catalys t	Ga-source	N-source (flow)	Supporting			Pressure (Torr)	Temperature (˚C)		diameter (nm)	length (μm)	
(Simpkins et al., 2006)	Ni-Fe alloy	Ga	NH_3 (20)	-	SiO_2/Si	CVD	atm	940	20	25~50	~10	-
(Hou and Hong, 2009)	Au	Ga	N_2	Ar used to transport Ga H_2 used to make (GaH_x) N_2 and H_2 total flow = 200	sapphire	plasma-enhanced CVD	2	900	120	60~90	-	-
(Wang et al., 2009)	Ni	Ga_2O_3	NH_3 (800)	-	Si	CVD	-	1100	40	50	10~20	-
(Chèze et al., 2010)	Ni	Ga	N_2	-	sapphire	MBE	-	730	3	-	-	Used advanced apparatus to study nucleation process.
(Kuo et al., 2011)	Ni, Au, Ni-Au alloy	$GaCl_3$, Ga_2Cl_4	NH_3 (100)	-	Si (100)	CVD	atm	900	30	Ni: 20~80	20~40	-
(Navamathavan et al., 2011)	Au	TMGa (3)	NH_3 (2000)	-	Si (111)	MOCVD	600 Torr	700 (to form Au-Ga alloy); 950 (growth)	60	80~150	1~3	-

Table 2.1: (Continued)

Ref.	Precursors				Substrate	Growth method	Growth ambient		Growth duration (min)	Size		Remarks
	Catalyst	Ga-source	N-source (flow)	Supporting			Pressure (Torr)	Temperature (˚C)		diameter (nm)	length (µm)	
(Shi and Xue, 2011)	Ni	Ga_2O_3	NH_3 (800 sccm)	-	Si (111)	CVD	-	1100	10,20,40, 60	20~50	10~30	-
(Diaz et al., 2012)	Au	TMGa	NH_3	-	porous polycrystalline Si (200 µm)	MOCVD (conceptually)	-	800	2	-	-	Experiment performed inside TEM, to study nucleation.
(Schuster et al., 2012)	-	Ga	N_2	-	type Ib diamond	Plasma-assisted MBE	ultra high vacuum	930	20~180	80	~0.5	-
(Avit et al., 2014)	Au-Ni alloy	Ga	NH_3	HCl to react with Ga N_2/H_2 carrier to dilute HCl	*c*-plane sapphire	HVPE	atm	800 (HCl-Ga reaction) 980 (growth)	30	70~200	~60 (or more)	Growth rate = 130 µm/h

All gases flow rate expressed in standard cubic centimetre per minute (sccm), otherwise stated.

Proper growth apparatus should be considered first prior to venturing towards growing GaN nanowires. From the table, it was showed that GaN nanowires could be grown using a variety of that, ranging from simple CVD setup, to the highly sophisticated molecular beam epitaxy (MBE) system (Seryogin et al., 2005, Kuo et al., 2011, Schuster et al., 2012). This flexibility had allowed growth apparatus to be individually tailored in light of achieving their respective objectives. For example, MBE system in general has lower growth rate, which suitable for real-time monitoring the nucleation and growth of nanowires (for in depth fundamental studies) with the aid of line-of-sight quadrupole mass spectrometry (QMS) and reflection high energy electron diffraction (RHEED) (Chèze et al., 2010). Although having precise control over growth rate might implied good nanowires quality, the cost of using MBE equipment was too expensive. Fortunately, a simple basic CVD setup was shown to be capable of fabricating nanowires of good structural quality, additionally displayed promising results in terms of electrical characteristics (Kim et al., 2006, Stern et al., 2005). In short, growth apparatus aimed to provide suitable ambient to nanowires fabrication. Given that such flexibility applied for them, the next step would be reviewing the growth ambient.

Despite wide flexibility in terms of fabrication tools, the growth temperature for GaN nanowires was slightly restricted. Although that from 730 to 1100˚C were reported; however, 900˚C and above would be more common (Cai et al., 2006, Djurišić et al., 2007, Xiao et al., 2009, Chèze et al., 2010). Still, there were an upper limit for growth temperature, where when it exceeds 1100˚C, GaN would be decomposed into Ga and N_2 (Xiao et al., 2007). Hence, it could be noted that the temperature window for GaN nanowires growth limited between 900 and 1100˚C. Meanwhile, other ambient aspects such as growth pressure seemed unlikely to be

restricted, since GaN nanowires could even be grown at atmospheric (atm) pressure (Stern et al., 2005, Kuo et al., 2011, Avit et al., 2014). This was done by vacuuming the growth chamber, subsequently introducing inert gases and sufficient amount of NH3 to raise the pressure. As most growth chambers utilized quartz tube, the vacuum pressure would be far from that in MBE, thus raising the concerns about oxygen (O)-related impurities. This was debunked by characterizing the electrical aspects such as carrier concentrations of the nanowires, which ultimately showing negligible differences between them (Stern et al., 2005). The notable changes observed, however, would be the nanowires yield, where their amount proportionated with growth pressure (Stern et al., 2005, Ra et al., 2010). Overall, the growth temperature range was limited, however, could be easily achieved with a suitable furnace. The less stringent rule on pressure allowed dynamic growth of nanowires.

Since apparatus and ambient have been chosen, the next step would be determining the growth parameters such as substrates, durations, and precursors that defined the physical aspects of the nanowires. For substrates, it was noteworthy that the first GaN nanowires synthesized in the absence of such (Han, 1997). Then, anodic alumina was used and probably considered as a substrate, despite being dissolved in the end (Cheng et al., 1999). Before the dawn of nanowires, sapphire (particularly *c*-plane) and silicon were well-known substrates for GaN thin film, although the latter required buffer layer due to poor lattice matching (Ambacher, 1998, Zhao et al., 2003, Xiao et al., 2009). Such idea had been implemented for nanowires growth, and surprisingly the results were positive, even in the absence of buffer layer (Seryogin et al., 2005, Zhang et al., 2006, Cai et al., 2006, Shi and Xue, 2011). Other than that, nanowires had also been grown on other substrates such as gallium arsenide (GaAs), quartz, and diamond (Stern et al., 2005, Li et al., 2006,

Gottschalch et al., 2008, Schuster et al., 2012). As for growth duration, so far, there were yet to be a conclusive study on that, while it was interesting to note even as low as one minute had been reported (Seryogin et al., 2005, Chèze et al., 2010, Diaz et al., 2012). However, to be practical for simple CVD setup, setting the growth duration about 30 minutes and above would ensure the grown nanowires being notable under an electron microscope (Cai et al., 2006, Lei et al., 2008, Kuo et al., 2011, Avit et al., 2014). On the other hand, the growth precursors would be discussed in the subsequent section, since they played an essential role in nanowires growth.

2.2 The Chemistry of GaN-related Precursors

GaN nanowires have been successfully synthesized occasionally. The precursors of GaN varied, sometimes depending on the growth apparatus, e.g. N_2 gas could serve as N-precursor to GaN in the presence of plasma system such as those in MBE (Kuo et al., 2008, Brandt et al., 2010). Then, for MOCVD, trimethylgallium (TMGa) would be used instead as opposed to Ga_2O_3 or Ga metal in simple conventional CVD systems (Ji et al., 2007, Ra et al., 2010). Meanwhile, HVPE employed corrosive precursors such as hydrogen chloride (HCl) in order to produce gallium (I) chloride (GaCl), an unstable compound and readily reacted with NH_3 to form GaN, although additional safety features to be heeded since the by-product such as ammonium chloride (NH_4Cl) could potentially clogged the exhaust (Molnar et al., 1997, Seryogin et al., 2005, Kuo et al., 2011). As this work employed simple conventional CVD setup, discussions would be focused Ga_2O_3, Ga metal, and NH_3.

Often, Ga metal was used solely in many conventional CVD GaN nanowires growth apparatus (Zhang and Zhang, 2002, Cai et al., 2006, Simpkins et al., 2006). However, the vapour pressure of Ga is 1×10^{-4} Torr (at 900˚C, which suitable for

GaN growth), thus the substrates have to be placed very near it to ease flux transportation to produce reasonable amount of nanowires (Han, 1997, Zhu and Fan, 1999, Stern et al., 2005). In addition, Ga metal tends to coagulate inwards, taking the form of droplets, which geometry limits the reaction area. This was mainly due to the formed GaN layers would inhibit the diffusion of N into the inner Ga, preventing additional flux to be generated (Kim et al., 2011). In order to increase the wettability of Ga, very small amount of bismuth was added (Kim et al., 2011). This however would introduce impurities to the overall growth process.

In light of the low vapour pressure of Ga metal, Ga_2O_3 powder was added to produce gallium suboxide (Ga_2O), which vapour pressure is four order greater than that of Ga (1 Torr at 900˚C), moreover existed in vapour state (Han, 1997, Zhu and Fan, 1999, Stern et al., 2005). This had allowed richer Ga-flux to be generated, allowing better interactions between substrate and NH_3 to obtain greater amount of nanowires. The compound of interest here would be Ga_2O, a reduced form of Ga_2O_3 that in so far as reported, could only be produced at high temperature. Various reducing agents such as Ga, hydrogen (H_2), and carbon (C) have been used, while the results were positive (Han, 1997, Zhu and Fan, 1999, Shin et al., 2008, Imade et al., 2010, Zervos and Othonos, 2010). In light of producing consistent amount of Ga_2O throughout the growth duration, H_2 would be much suitable; in addition, able to react with residue oxygen (O_2) in the growth chamber, reducing of O-related impurities within the nanowires (Imade et al., 2010, Wright et al., 2010). H_2 could be prepared by channeling it to the growth chamber from a tank, or derived from NH_3 (Ji et al., 2007, Hou and Hong, 2009, Davidson et al., 1990, Monnery et al., 2001, Ganley et al., 2004).

NH_3 had been widely used as an N precursor for GaN synthesis compared to N_2. Between them, the latter was held by N-N triple bond that required tremendous energy to break, and currently only dedicated plasma systems were capable of such task (Schuster et al., 2012). NH_3, on the other hand, consisting of three N-H bonds that could be easily broken compare to that of N_2. Since then, it was believed that the dissociated NH_3 species were capable of reacting with Ga_2O to yield GaN.

The decomposing mechanism of NH_3, resulted in dissociated ammonia, was rather intriguing, since the actual ones comprised of many steps, moreover complicated. However, they could be summarized as shown from Eqn. (2.1) to (2.5) (Ganley et al., 2004). For better representation of NH_3 and its dissociated component, NH_x, where $x = 0, 1, 2, 3$ would be referred to.

$$NH_3 \rightarrow NH_2 + H \qquad (2.1)$$

$$NH_2 \rightarrow NH + H \qquad (2.2)$$

$$NH \rightarrow N + H \qquad (2.3)$$

$$N + N \rightarrow N_2 \qquad (2.4)$$

$$H + H \rightarrow H_2 \qquad (2.5)$$

Hence, the overall reaction of NH_3 decomposition would be as shown in Eqn. (2.6) (Monnery et al., 2001, Wang et al., 2008, Qin et al., 2008a).

$$2NH_3(g) \rightarrow N_2(g) + 3H_2(g) \qquad (2.6)$$

The products from the decomposition were rather surprising. While H_2 could serve as reducing agent for Ga_2O_3 to generate Ga_2O, as shown in Eqn. (2.7), N_2 remained unreactive towards Ga_2O (Collins et al., 2005, Xu et al., 2006, Qin et al., 2008a, Jung, 2013).

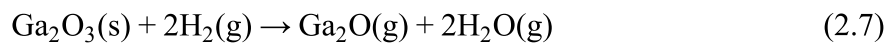

$$Ga_2O_3(s) + 2H_2(g) \rightarrow Ga_2O(g) + 2H_2O(g) \qquad (2.7)$$

Fortunately, the conversion rate seen in Eqn. (2.6) to its final products was slow; furthermore fresh NH_3 gradually channeled into the chamber during growth, thus sufficient to form GaN.

By taking into account about Ga_2O reacting with either NH_3 or its dissociated species, a global equation was proposed and expressed in Eqn. (2.8) (Xu et al., 2006, Qin et al., 2008a, Imade et al., 2010, Jung, 2013):

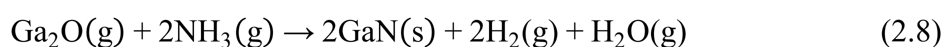

$$Ga_2O(g) + 2NH_3(g) \rightarrow 2GaN(s) + 2H_2(g) + H_2O(g) \quad (2.8)$$

The overall reactions revealed desorption of hydrogen related species such as H_2 gas and water vapour (H_2O) has occurred, indicating the presence of NH_3 dissociation. Therefore, it could be concluded that regardless of the form NH_3 had undertaken, the scission of (nitrogen-hydrogen) N-H bonds were necessary in order to form GaN.

2.3 The Growth Modes of GaN Nanowires

In general, there were two modes for 1D nanostructure (such as GaN nanowires) growth, namely vapour-solid (VS) and vapour-liquid-solid (VLS) growth. One distinguishable aspect between them would be the presence of metal particles that served as catalyst in VLS growth, while absent in VS (Rao et al., 2003).

In VS growth, vapour phase reactants generated from precursors would be selectively condensed on a substrate surface first to form nuclei, subsequently absorbing the incoming reactants to trigger one dimensional (1D) growth (Consonni et al., 2010). The selective condensation process at times proved to be challenging, hence patterned mask such as anodic alumina membrane and silicon oxide (SiO_x) have been employed (Cheng et al., 1999, Zhang and Zhang, 2002). In recent development, VS growth could be achieved in the absence of the aforementioned, by

controlling the deposition rate to induce seed nucleation. Such task was commonly done using MBE system (Calarco and Marso, 2007, Brandt et al., 2010, Tourbot et al., 2011).

VLS growth offered greater flexibility in regardless of growth apparatus, and had higher chances of triggering nanowires growth. This mechanism was firstly demonstrated by Wagner and Ellis (1964) for the growth of Si nanowires, with Au nanoparticles as catalyst. According to them (as shown in Figure 2.1), the VLS growth could be described where Au nanoparticles absorbing Si reactants from vapour phase silicon tetrachloride ($SiCl_4$), forming Au-Si alloy that existed in molten state. Continuous absorption eventually saturating the alloy droplet; hence excess Si will precipitate downwards, initiating 1D growth. In a prolonged duration with continuous supply of $SiCl_4$ will lead to the formation of Si nanowires. The concept of VLS growth was well-received, and in the later years, various metal catalysts have been investigated and proved to be suitable for 1D nanostructures growth.

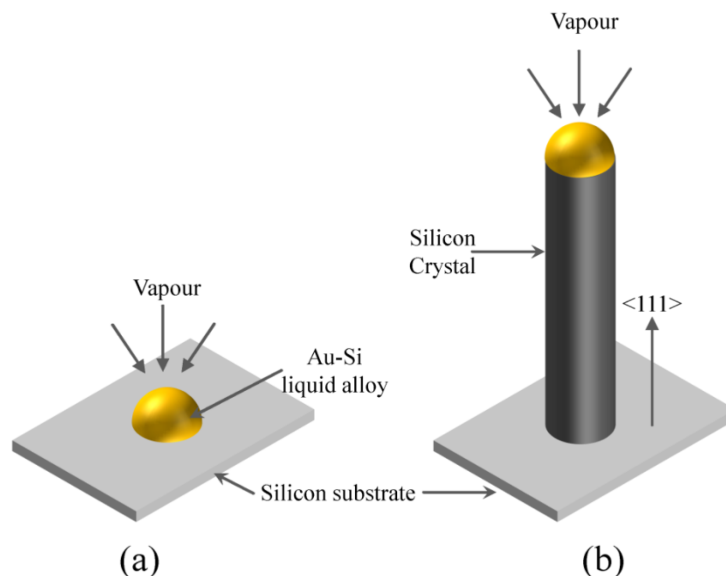

Figure 2.1: VLS growth of Si nanowire, (a) absorption and formation of liquid Au-Si, (b) growth of Si nanowire. Adapted and redrawn from Wagner and Ellis (1964).

In case of GaN nanowires, various metal catalysts have showed promising results in terms of growth such as Fe, Au, Ni, and indium (In), as listed in Table 2.1. Among them, Au and Ni seemed to receive great attentions. Although many works have been done, majority of the proposed growth mechanism was cursory. The challenge here lied within the alloying stage of VLS mechanism, where the interactions of gallium (Ga) and nitrogen (N) with the catalyst still unclear. Taking Ni as example, it was proposed that a ternary compound, such as Ni-Ga-N would be formed and existed in liquid state (Wang et al., 2009, Xue et al., 2009, Qin et al., 2008a, Qin et al., 2008b). However, Chèze et al. (2010) observed otherwise, where Ni-Ga would be preferably formed first, followed by N dissolving into Ni-Ga, precipitating GaN when sufficient Ga and N had been absorbed. Besides that, Diaz et al. (2012) also reported similar case, where Au was used as catalyst instead. These results implied that Ga and N could independently alloyed with the catalyst, and GaN nanowires could still be precipitated as long as sufficient Ga and N have been dissolved to saturate the catalyst. Although the aforementioned results were very significant in terms of in depth understanding of GaN nanowires growth, still, the mechanism could be affected by varying the parameters (Zhang et al., 2006, Ra et al., 2010). Nevertheless, it was believed that the growth characteristics of GaN nanowires could be fine-tuned by controlling the alloying process.

2.4 General Characteristics of GaN Nanowires

This section described some of the characteristics of GaN nanowires. Here, only those grown on substrate would be referred and discussed. Firstly, the nanowires samples appeared as a light yellowish cotton layer, which often reported (Qin et al., 2009, Cui et al., 2014, Shi and Xue, 2011). Interestingly, the colour was

similar to that of GaN powder; however, that of darker yellow tone implied lesser O-impurities, and in the purest state GaN appeared as greyish colour (Kim et al., 2011, Roehrens et al., 2010). It should be noted that, the colour observation method being qualitative instead of quantitative; in addition, such would not be applicable for GaN thin film.

The crystal structure of GaN nanowires had been revealed to be hexagonal wurtzite most of the times, which belonged to the space group C_{6v}^{4} (Kuball, 2001, Harima, 2002). Determination of crystal structures could be done using XRD, high-resolution transmission electron microscopy (HRTEM), and Raman spectroscopy methods (Liu et al., 2001, Zhang and Zhang, 2002). Among them, XRD could provide the diffraction pattern in terms of angles, which method known as 2θ phase analysis. Then, such pattern would be identified by referencing to International Center of Diffraction Data-Powder Diffraction File (ICDD-PDF) cards (Jung, 2012). Meanwhile, HRTEM could be used to determine the interatomic spacing visually (Shi et al., 2011). Since that being unique for each material, identifications were simplified.

GaN, being in the space group C_{6v}^{4}, has eight sets of Raman modes at the Γ point that can be expressed as $\Gamma = 2A_1 + 2E_1 + 2B_1 + 2E_2$. While one set of A_1 and E_1 modes being acoustic; the rest were optical, which would display themselves in typical Raman measurement (Kuball, 2001, Harima, 2002). Between GaN thin film and nanowires, their Raman spectra exhibited one discernible difference in terms of full-width at half-maximum (FWHM), or linewidth of the Raman bands. In general, the latter being broader than the former due to finite size effects (Liu et al., 2001). This feature was also significant when the nanowires were characterized using photoluminescence (PL) spectroscopy, particularly at the band emission (~3.4 eV)

(Chin et al., 2007). As a result, the bands (either from Raman or PL) at times would be superimposed, and required mathematical approach to separate them, subsequently obtaining empirical information regarding such. The general models, frequent used for such were Gaussian and Lorentzian (Bouguerra et al., 2008, Robins et al., 2007, Dhara et al., 2011). A more detailed discussion regarding these would be presented in the later chapters.

2.5 Porous GaN (PGaN) Fabrication Process

When GaN thin film was subjected to chemical etching, under certain conditions, porous surface could be obtained. Such surface have been studied and revealed to hold importance in thin film fabrication. With its morphological aspects, the treated GaN surface was commonly referred as PGaN.

In general, PGaN surface housed many pore networks, thus having a greater exposed area than that of regular thin film. Clearly, an increased in surface area would allow higher sensitive sensors to be made, such as gas sensors (Yam and Hassan, 2007, Ramizy et al., 2011). However, the more important aspect would be the characteristics brought about by PGaN, which was attaining stress relaxation (Vajpeyi et al., 2005, Soh et al., 2007, Vajpeyi et al., 2007). Typical GaN thin film grown on sapphire tends to have growth defects such as threading dislocation, in the order of 10^{8}~10^{10} cm^{-2} that being the bane of device performances (Youtsey et al., 1997, Liu et al., 2009, Zhang et al., 2010). Through the fabrication of PGaN, selected GaN grains would be etched away, leaving a stress relieved layer. Subsequent thin film grown on such layer, now acting as buffer, would eventually lower the overall defects (Mynbaeva et al., 2005, Soh et al., 2007, Wang et al., 2010).

It was known that various methods have been developed for fabricating PGaN, among them would be dry and wet etching. Dry etching of GaN involved sophisticated apparatus such as inductive coupled-reactive ion etching (ICP-RIE) that used corrosive gases such as chlorine as etchant, while to obtain a porous morphology, certain areas of GaN should be covered through a patterned mask (Pearton et al., 1999, Wang et al., 2010). The process was tedious; hence wet etching was opted instead.

Wet etching of GaN received much attention due to flexible yet simple experimental setup; moreover attain control over various parameters. In general, this method can be further divided into two categories, namely chemical bath immersion and electrochemical process (Zhuang and Edgar, 2005). The former could be done by immersing the GaN sample into a chemical bath, either consisted of aqueous or molten salt that above room temperature. This resulted in specific etched profiles such as hexagonal pits that implied defective area. However, such technique excels in studies of defects, but unable to deliver high amount of porous structure (Zhang et al., 2010).

Meanwhile, electrochemical etching could be divided into that of electroless or anodic (Zhuang and Edgar, 2005). One common aspect for them would be the establishment of electrical connections between the GaN sample and an inert electrode such as platinum (Pt). Typical electroless process adapts a galvanic cell configuration, where the resultant reactions depended on their respective electrode potential (Minsky et al., 1996, Youtsey et al., 1997). Meanwhile, an external source, usually constant voltage was applied between GaN and Pt for the anodic process (Seo et al., 2001). To further enhance the electrochemical reactions, UV light illumination was often included, in light of the ability of GaN to photogenerate

electron-hole pairs (Minsky et al., 1996, Youtsey et al., 1997, Seo et al., 2001). These methods thus become well-known and often termed as "photoelectrochemical (PEC) etching" in literature.

The first PEC process was introduced by Minsky et al. (1996) and being compared to that of GaAs in order to deduce the possible mechanism. (Youtsey et al., 1997) used mercury (Hg) arc lamp as UV source (where experimental setup is shown in Figure 2.2) to produce moderate light intensities [greater than reported by Minsky et al. (1996)] and such resulted in highly anisotropic etch profile of GaN on 6H silicon carbide (SiC).

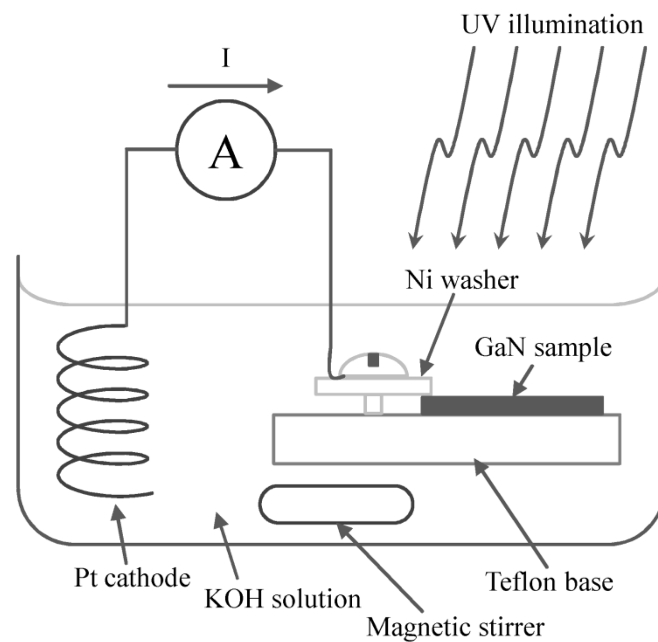

Figure 2.2: Electroless PEC setup. Adapted and redrawn from Youtsey et al. (1997).

Although less emphasized, long and straight vertical pore channels were observed in their micrographs. The directional etching characteristics from the aforementioned had implied porous morphology could be obtained and retained up to several micrometers, which would be advantages for various applications. However,

Seo et al. (2001) revealed that etching could not be commenced in the absence of an external bias when electrolytes aside from the typical potassium hydroxide (KOH) was used. This had illustrated the limitation of electroless etching. By taking into account with the aforementioned concerns and implementing new experimental conditions, GaN with high pore density with definable channels was successfully fabricated in the subsequent years (Díaz et al., 2002, Díaz et al., 2003, Vajpeyi et al., 2005, Vajpeyi et al., 2009, Yam et al., 2007).

2.6 Introduction to NH_3 Gas Sensor

NH_3 is widely known for its pungent smell and corrosiveness in nature. In general, such gas could be found in farms, automotive industries, chemical processing plants, and medical field (Timmer et al., 2005). It was known that the amount of NH_3 produced and consumed varied accordingly, and could prove fatal should it be handled recklessly. Hence, NH_3 gas sensors were made and placed in strategic sites.

To date, there were many types of gas sensors being studied. In relation to this work, only those GaN based would be focused upon. For sensor fabrication, a typical yet simple design of that would involve deposition of electrical electrodes on GaN layer that acted as the sensing material (Luther et al., 1999, Lee et al., 2003, Chen et al., 2011). Being a metal-semiconductor-metal configuration, the resulting electrical behaviour, as referred from the current-voltage (I-V) profile, could be either Schottky (rectifying) or Ohmic (linear) (Weng et al., 2009, Chen et al., 2011). In most sensors, corrosion resistance metals such as Au, Pt, palladium (Pd), and (iridium) Ir were often used since they remained inert towards the sensed gas (Gu et al., 2012). Given that some of the electrodes may have a higher metal work function